

# Quantitative Analysis of Skin using Diffuse Reflectance for Non-invasive Pigments Detection

Shiwei Li<sup>1</sup><sup>a</sup>, Mohsen Ardabilian<sup>1</sup><sup>b</sup> and Abdelmalek Zine<sup>2</sup><sup>c</sup>

<sup>1</sup>Ecole Centrale de Lyon, LIRIS CNRS, France

<sup>2</sup>Ecole Centrale de Lyon, ICJ CNRS, France

**Keywords:** Artificial Neural Networks, Biomedical Engineering, Bioinformatics, Biomedical Signal Processing.


**Abstract:** Skin diagnosis has become a significant part of research topics in biomedical engineering and informatics, since many conditions or symptoms of diseases, such as melanoma and jaundice, are indicated by skin appearance. In the past, an invasive method (i.e. Biopsy) is widely used for pathological diagnosis by removing a small amount of living tissue. Recently, non-invasive methods have been studied based on diffuse reflectance for detecting skin inner information. With the development of machine learning techniques, non-invasive methods can be further improved in many aspects, such as the speed and accuracy. Our research focuses on analyzing and improving non-invasive skin pigments detection using neural networks. The relation between skin pigments content and skin diffuse reflectance has been studied. Moreover, the computational time has been accelerated significantly after using the inverse mapping neural network instead of the forward mapping one. The results show that our proposed method can obtain favorable results in estimating melanin content, blood content, and oxygen saturation from synthetic skin diffuse reflectance for all lightly, moderately, and darkly pigmented skin types compared to Monte Carlo simulations. And it turns out that our method works well when using a measured skin reflectance database from National Institute of Standards and Technology for the second validation.


## 1 INTRODUCTION


Skin, one of the most important human body organs, protects us from external invasion, keeps us warm, and regulates the balance of water. Skin health has become a significant issue. For example, there have been many computer vision-based tasks which focus on analyzing different facial features (Leo et al., 2020). Some diseases reflect the abnormal content of the pigment inside the skin, for instance, melanoma is caused by a large amount of melanin produced by exposure to sunlight. To give an intuitive and quantitative expression, evaluating pigments content is required. Traditional method for pigments detection is examined under a microscope or analyzed based on a series of chemical processes by taking a small skin sample from the individuals, and is called biopsy (Zerbino, 1994). As skin appearance can be affected by many pigments, such as melanin, hemoglobin, etc., researchers found that

light waves can penetrate the skin, and the outgoing wave (also called diffuse reflectance) which is scattered back, carries the inner information. In the past two decades, the non-invasive detection of pigments deposited inside the skin has progressed based on skin diffuse reflectance. Combined with skin models, light-skin interaction approaches are applied to analyze skin diffuse reflectance monitored by diffuse reflectance spectroscopy (DRS) instruments and obtain the pigments content. These light-skin interaction approaches describe how light transports inside the tissue, and derive diffuse reflectance based on the optical parameters of skin models, which generally are formed as a function of volume fractions of skin pigments. With the development of DRS techniques and hyper-spectral sensors, the acquisition of diffuse reflectance with high resolution (usually 1-20 nm) becomes easier and cost-effective. These techniques have been applied to diagnose skin diseases, etc. (Mazzoli et al., 2010; Mehrübeoğlu et al., 2002; Salomatina et al., 2006; Wallace et al., 2000).

Light-skin interaction approaches have been studied and improved over the past four decades, such as diffuse approximation (DA), kubelka-munk theory,

<sup>a</sup> <https://orcid.org/0000-0002-8765-9283>

<sup>b</sup> <https://orcid.org/0000-0002-1842-0404>

<sup>c</sup> <https://orcid.org/0000-0002-0353-8995>

and Monte Carlo simulations (MC) (Sharma et al., 2014; Zonios et al., 2008; Vyas et al., 2013; Ishimaru, 1978). Besides, machine learning methods have also been applied more commonly to map diffuse reflectance and skin physiological parameters (Zhang et al., 2010; Chen et al., 2016). Among these approaches, MC is mostly used to validate other approaches as the first verification because it simulates the movement of energy packets that obey radiative transport rules and has a good fitting performance with the measured data (Jacques, 1996). Fredriksson, Larsson, and Strmberg presented a 3-layered analysis model based on MC which is able to estimate micro circulatory parameters (Fredriksson et al., 2012). Sharma *et al.* proposed a 2-layered lookup table based on MC, which is generalized to be used for a wide variety of probe-geometries with the error of absorption properties varying from 12 to 25% (Sharma et al., 2014). Nonetheless, MC accelerated by GPU (Alerstam et al., 2008) needs around a day to run the curve-fitting process for only one hyper-spectral diffuse reflectance. With this in mind, it is inefficient when processing amounts of diffuse reflectance spectra data and cannot satisfy the demand to extract skin physiological parameters rapidly. DA is known to be a second-order differential equation that gives approximate solutions of the Boltzmann transport equation on the basis of spherical harmonics. Spott and Svaasand focused on collimated light sources in turbid media and proposed a hybrid approach by refining the source terms or increasing the approximation order in DA (Spott and Svaasand, 2000). Nagli *et al.* tested the suitability of DA for fitting the diffuse reflectance spectra and extracting bio-parameters from human skin in vivo (Naglič et al., 2019). DA assumes that the scattering dominates light-skin interaction over the absorption and is much faster than MC. However, its not appropriate when light source is near the interface of skin tissue (Furutsu, 1980) or the tissue is highly anisotropic and lowly scattered (Zherebtsov et al., 2019). Yudovsky and Pilon developed a semi-empirical model to relate the diffuse reflectance to the radiative properties and thickness of 2-layered media [18,19]. However, this model is limited to that the scattering must be strongly forward. Zonios *et al.* found that the optical absorption spectrum of in vivo melanin exhibits an exponential dependence on wavelength and presented a new method for studying melanin but is assumes skin is a homogeneous semi-infinite medium with one layer (Zonios et al., 2008). The empirical models usually have many restrictions, which means the feasibility and the practicability are not enough for applications. Recently, with the development of machine learning and deep learning, support vector regression, artificial neural

networks, etc. have been applied in this domain frequently. Yudovsky, Nguyen, and Durkin simulated spatial frequency domain reflectance of skin for multiple wavelength with a forward neural network and found that the optical properties could be determined independently with minimal coupling (Yudovsky and Durkin, 2011; Yudovsky et al., 2012). This modeling method is not only precise but also robust (Tsui et al., 2018) when dealing with the reflectance collected by a separated source detectors system, however, it suffers from some limitations, for example, fixing the thickness of skin layers. The inverse neural network is also applied to solve the problem, which is faster than forward neural network but with large prediction errors (Wang et al., 2012). There are still many potentials in applying neural networks to detect skin physiological parameters.

Two categories have been designed based on the mapping directions. The forward one is to map skin physiological parameters to skin diffuse reflectance, and the inverse one is the reverse. We have built a 3-layered skin model composed of 12 parameters and generated a skin diffuse reflectance database using MC. This database, which contains 50000 samples to avoid overfitting, was then used for training a forward mapping neural network (FNN). Afterward, we tested the performance of FNN compared with MC in three skin types. In total 30 samples from lightly pigmented to darkly pigmented were created with the help of MC and then used for the first validation. The measured skin reflectance database was used for the second validation. Moreover, an inverse mapping neural network (INN) was also proposed and studied in our research for speeding up the detection of melanin content. Our research aims at: 1) applying both FNN and INN in non-invasively extracting melanin, hemoglobin, etc. based on DRS; 2) analyzing the effects of skin physiological parameters on reconstructing skin diffuse reflectance; 3) testing the suitability of neural networks when dealing with three different skin types.

## 2 METHODOLOGY

### 2.1 Skin Model

For quantitative analysis of skin, we first need to build a skin model. Human skin is a multi-layered biological tissue, which generally is divided into three layers: the epidermis, the dermis, and the subcutis. These three layers can be detailed with many sub-layers. To our best knowledge, a maximum 9-layered skin model has been researched by refining the epidermis and the dermis which consists of stratum corneum,

stratum granulosum, stratum basal, papillary dermis, subpapillary dermis, upper blood net dermis, reticular dermis, deep blood net dermis, and subcutis (Maeda et al., 2010). Although a complex structure contains more information, it increases the computational time especially using MC. In our research, a 3-layered model including the epidermis, the dermis, and the subcutis is taken into account.

Skin appearance is mainly influenced by the optical properties of each layer. Following this, we defined each layer with thickness, absorption coefficient, scattering coefficient, refractive index, and anisotropic factor. The thickness of the epidermis varies from 0.027 to 0.15 mm (Baranoski and Krishnaswamy, 2010). Light propagating in this layer is absorbed mostly by melanin, which is a common natural biological pigment. There are two types of melanin, of which the absorption spectra are not identical. Eumelanin and pheomelanin exhibit differences in color. The absorption coefficient of the epidermis can be explained as a linear wavelength-dependent function as:

$$\begin{aligned} \mu_{a,epi} = & C_m * (\mu_{a,phéo} * \beta + \mu_{a,eu} * (1 - \beta)) \\ & + C_{w,epi} * \mu_{a,w} + (1 - C_m - C_{w,epi}) * \mu_{a,base} \end{aligned} \quad (1)$$

where  $C_m$  and  $C_{w,epi}$  represent the volume fraction of melanin and water in the epidermis;  $\beta$  is the ratio between pheomelanin and eumelanin;  $\mu_{a,phéo}$ ,  $\mu_{a,eu}$ , and  $\mu_{a,w}$  are the absorption coefficient of pheomelanin, eumelanin, and water respectively; the absorption of skin baseline  $\mu_{a,base}$  is an approximation given by (Jacques, 1996) and it can be considered as the absorption of collagen fibers inside skin without any skin pigments.

The dermis is composed of dense, irregular connective tissue, and blood vessels. The thickness of the dermis is from 0.6 to 3 mm (Baranoski and Krishnaswamy, 2010). The dominant pigment in this layer is hemoglobin in the blood. Hemoglobin can also be divided into two types based on if it is oxygenated. The absorption spectra of oxy-hemoglobin and deoxy-hemoglobin differ clearly in the visible light range. The absorption coefficient of the dermis is a weighted combination of the primary hemoglobin absorption and the minor absorption of skin baseline and water, given by:

$$\begin{aligned} \mu_{a,der} = & C_{bl,der} * (\mu_{a,oxy} * S + \mu_{a,deoxy} * (1 - S)) \\ & + (1 - C_{bl,der}) * C_{w,der} * \mu_{a,w} \\ & + (1 - C_{bl,der}) * (1 - C_{w,der}) * \mu_{a,base} \end{aligned} \quad (2)$$

where  $C_{bl,der}$  and  $C_{w,der}$  are the volume fraction of blood and water in the dermis;  $S$  indicates the oxygen saturation in the blood;  $\mu_{a,oxy}$  and  $\mu_{a,deoxy}$  stand for the absorption coefficient of oxy-hemoglobin and

deoxy-hemoglobin respectively considering the concentration of hemoglobin in the blood.

Lastly, the subcutis is assumed to be an up to 5 mm thick tissue. The absorption elements in the subcutis include blood, fat, water, and skin baseline. The absorption coefficient of this layer is similar to the dermis by adding the extra absorption of fat, given by:

$$\begin{aligned} \mu_{a,sub} = & C_{bl,sub} * (\mu_{a,oxy} * S + \mu_{a,deoxy} * (1 - S)) \\ & + (1 - C_{bl,sub}) * C_{fat} * \mu_{a,fat} \\ & + (1 - C_{bl,sub}) * (1 - C_{fat}) * C_{w,sub} * \mu_{a,w} \\ & + (1 - C_{bl,sub}) * (1 - C_{fat}) * (1 - C_{w,sub}) \\ & * \mu_{a,base} \end{aligned} \quad (3)$$

Note that all absorption coefficients of skin pigments are taken from in vivo experimentation (Jacques and Prahl, ). And for (2) and (3), we introduced a mathematical method residual volume fraction to avoid that the sum of volume fractions of all pigments surpasses 1. We assume that  $\mu_a^i$  is the absorption coefficient of the  $i$ -th pigment with the volume fraction  $C_i$  in one layer. Then, the absorption coefficient of this layer  $\mu_{a,layer}$  is generally defined as a linear form:

$$\begin{aligned} \mu_{a,layer} = & \sum_{i=1}^n \mu_a^i C_i + (1 - \sum_{i=1}^n C_i) \mu_{a,base} \\ \text{s.t. } & \sum_{i=1}^n C_i < 100\% \end{aligned} \quad (4)$$

where  $n$  is the total number of pigments types in this layer. However, when  $n$  is too large, it's quite normal that the condition can not be satisfied. That's why we introduce residual volume fraction. And the modified equation is shown as:

$$\mu_{a,layer} = \sum_{i=1}^n \left[ \prod_{j=1}^{i-1} (1 - C_j) \right] C_i \mu_a^i + \prod_{i=1}^n (1 - C_i) \mu_{a,base} \quad (5)$$

Besides the absorption, the scattering events occur massively inside skin. To define these events, Rayleigh scattering and Mie scattering are commonly used in skin optics. The scattering coefficient is fit with an equation to match those experimentation results according to (Jacques, 2013):

$$\begin{aligned} \mu_s = & \mu_{s500(nm)} * (f_{Ray} * (\frac{\lambda}{500(nm)})^{-4} \\ & + (1 - f_{Ray}) * (\frac{\lambda}{500(nm)})^{-b_{Mie}}) \end{aligned} \quad (6)$$

where  $\mu_{s500(nm)}$  is the scattering coefficient measured at 500 nm;  $f_{Ray}$  indicates the fraction of Rayleigh scattering, and clearly  $1 - f_{Ray}$  is that of Mie scattering;  $b_{Mie}$  is called the scattering power which is acquired by fitting the measured data.

The refractive index ( $n_{epi}$ ,  $n_{der}$ ,  $n_{sub}$ ) and the anisotropic factors ( $g_{epi}$ ,  $g_{der}$ ,  $g_{sub}$ ) of each layer are fixed as 1.44, 1.37, 1.37 and 0.8, 0.86, 0.75 respectively. All parameters in skin model are given in Table. I with descriptions and ranges.

## 2.2 Monte Carlo Simulations

With a well-defined skin model, we then implemented MC for reconstructing skin diffuse reflectance. The MC was coded in Python v3.6.4, following the manual of MCML (Wang et al., 1995). Fig. 1 shows the detailed flowchart of MC. To speed up the computational time, we reduced trigonometry operations by creating an array for indexing which directly stores the results. And GPU techniques were then applied to accelerate MC with almost 1000 times faster (Fang and Boas, 2009). For each simulation,  $1E07$  energy packets (or photons) were emitted perpendicular to the interface of tissue. Detection window was set as a circle with a radius 2 cm to ensure the total diffuse reflectance. The optical properties of tissue were calculated and set based on our 3-layered skin model. 50000 samples were simulated using MC by randomly defining 12 skin physiological parameters and the wavelength in the range from 450 to 700 nm. It took in total 18.2 hours for generating the skin reflectance database with Intel Core i7-7700HQ CPU and Nvidia GeForce GTX1060 GPU.

## 2.3 Neural Networks

Two neural networks have been built in our research with opposite mapping directions using the Deep Learning Toolbox in MATLAB R2018a. They are both composed of two hidden layers with 55 neurons (Tsui et al., 2018), one input layer and one output layer. For FNN, the inputs are the optical parameters of skin model with nine dimensions (e.g.  $\mu_{a,epi}$ ,  $\mu_{a,der}$ ,  $\mu_{a,sub}$ ,  $\mu_{s,epi}$ ,  $\mu_{s,der}$ ,  $\mu_{s,sub}$ ,  $d_{epi}$ ,  $d_{der}$ , and  $d_{sub}$ ) and the output is skin diffuse reflectance at one specified wavelength. For INN, the input is skin diffuse reflectance spectrum from 450 to 700 nm and the output are the volume fractions of skin pigments. The training function was set as the scaled conjugate gradient method. Besides this, normalization and random data division were applied to databases. Note that the database generated by MC was applied for training FNN, and another database generated with the help of FNN was then applied for training INN since MC needs a significant amount of time to reproduce the reflectance spectrum, and FNN provides very similar results to MC and works much faster than MC.

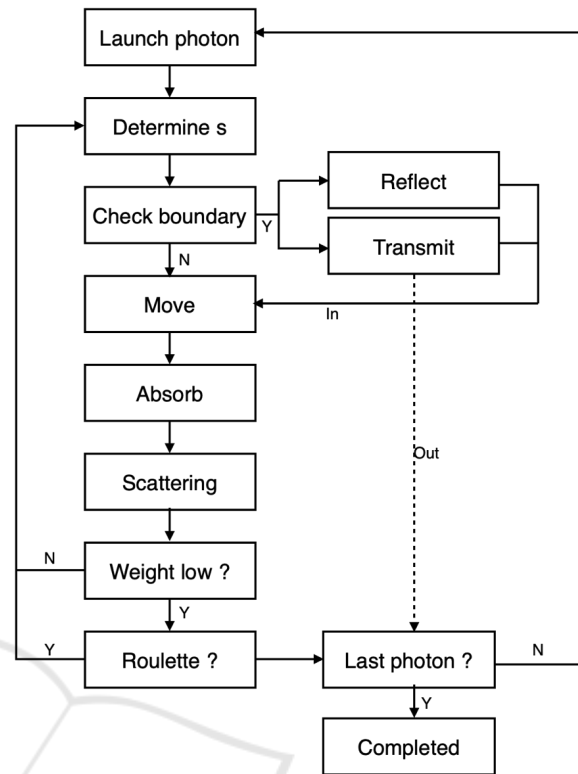


Figure 1: Flowchart of Monte Carlo simulations: energy packets are considered as photons with an initial weight 1.

## 3 EXPERIMENTATION AND RESULTS

The FNN was trained using the database generated by MC based on 3-layered skin model. Fig. 2 shows the performance which is the mean squared error during the training process. As illustrated, the error decreases dramatically at the start, then it tends to fall smoothly after 5000 epochs, and eventually, it holds steady. After FNN training was completed, the diffuse reflectance can be reproduced by predefining skin physiological parameters. Then we tested FNN on the performance of reconstructing skin diffuse reflectance. Taking pigmented degree into account, we sampled 10 times for lightly, moderately, and darkly pigmented in turn. The volume fraction of melanin varies from [1.3% 3%], [11% 16%], and [18% 43%] respectively (Jacques et al., 1996). 30 samples in total were created consequently. Starting from the same randomly assigned 12 parameters of skin model, FNN and MC reconstructed skin diffuse reflectance in the range from 450 to 700 nm. As can be seen in Fig. 3, the reconstructed diffuse reflectance curve gradually increases in the range from 450 to 500 nm, and a W pattern comes out from 500 to 600 nm. This is due



Table 1: Descriptions, symbols, and ranges of parameters in skin model.

Symbol	Description	Range
$C_m$	volume fraction of melanin	1.3-43% (Jacques, 1996)
$\beta$	ratio of pheomelanin to eumelanin	4.9-36% (Parsad et al., 2003)
$C_{w\_epi}$	volume fraction of water in epidermis	10-20%
$d_{epi}$	thickness of epidermis	0.027-0.15mm (Baranoski and Krishnaswamy, 2010)
$C_{bl\_der}$	volume fraction of blood in dermis	0.2-7% (Flewelling, 2000)
$C_{w\_der}$	volume fraction of water in dermis	40-90%
$S$	oxygen saturation	50-95% (Angelopoulou, 2001)
$d_{der}$	thickness of dermis	0.6-3mm (Baranoski and Krishnaswamy, 2010)
$C_{bl\_sub}$	volume fraction of blood in subcutis	5-20%
$C_{w\_sub}$	volume fraction of water in subcutis	40-90%
$C_{fat}$	volume fraction of fat	40-70%
$d_{sub}$	thickness of subcutis	1-5mm

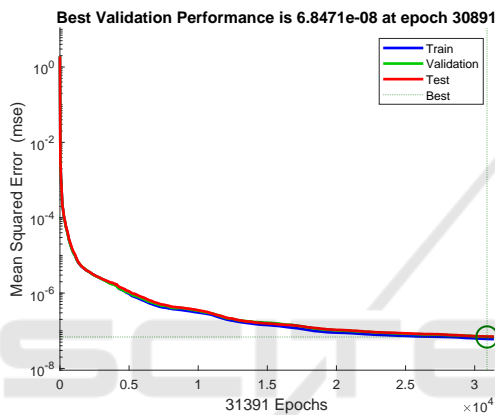


Figure 2: Performance for FNN trained by the MC database.

to the unique absorption of oxy-hemoglobin. Here, for sample no.1, the oxygen saturation in the blood is 65.1%. Generally, the higher the volume fraction of blood and oxy-hemoglobin, the more apparent this W pattern. When melanin dominates the absorption, the "W" pattern is no longer apparent. The root mean squared relative error (RMSRE) was used for evaluating the fitting performance, given by:

$$RMSRE = \sqrt{\frac{\sum_{\lambda=450nm}^{\lambda=700nm} (R_{\lambda} - T_{\lambda})^2}{N_{\lambda}}} \quad (7)$$

where  $R_{\lambda}$  and  $T_{\lambda}$  are respectively the diffuse reflectance produced by our method and the target reflectance;  $N_{\lambda}$  is number of wavelengths (bands), equaling 251 in our research. Then the RMSRE were calculated for all 30 samples in different groups. The average values of RMSRE using FNN are 0.0033, 0.0037, and 0.0061 for three groups. It turns out that FNN can yield skin diffuse reflectance extremely close to the target reflectance simulated by MC starting from the same skin physiological parameters.

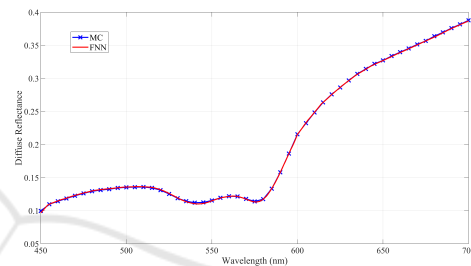


Figure 3: Reconstructing skin reflectance by MC and FNN: sample no.1.

### 3.1 Effects Analysis of Skin Parameters on Reconstructing Reflectance

Before detecting pigments information, we would like to first analyze the effects of skin parameters on reconstructing skin diffuse reflectance. One parameter is analyzed by varying its value while all other parameters are fixed. All parameters are initialized as the lower limit in Table. I.

The volume fraction of melanin is set from 1.3 to 43% with 2% increment in turn. Fig. 4(a) shows the results of reconstructing diffuse reflectance with varying  $C_m$ . We find that in general the reflectance decreases when  $C_m$  increases. The reflectance curve tends to be more flattened, and typical W pattern becomes less evident. The absorption coefficient of melanin decreases gradually and steadily over 450-700 nm. Accordingly, the diffuse reflectance increases gradually and steadily while  $C_m$  is too large and melanin dominates the absorption. Changing  $\beta$  does not really affects the shape of reflectance curve as shown in Fig. 4(b) since two types of melanin have similar absorption spectra in the visible light range, and  $\mu_{a\_pho}$  is slightly smaller than  $\mu_{a\_eu}$ . When  $\beta$  increases, the proportion of pheomelanin increases, thus, the total absorption caused by melanin decreases

a little. Consequently, the diffuse reflectance grows. The difference between  $\mu_{a.pheo}$  and  $\mu_{a.eu}$  becomes larger in long wavelength range. This is also reflected in the reconstructed diffuse reflectance, where the difference in long wavelength range is more evident.

The absorption of blood is mainly expressed as hemoglobin and oxygen saturation. Fig. 4(c), Fig. 4(d), and Fig. 4(e) illustrate the effects of blood in the dermis and subcutis, and oxygen saturation on reconstructing skin diffuse reflectance. With the volume fraction of blood increasing both in the dermis and subcutis, skin reflectance decreases. Moreover, the effects of blood in the dermis are more significant than in the subcutis since only small parts of light can penetrate into the subcutis and the long-wavelength light has better penetration. That's why the effects of blood in the subcutis mainly locate in the range from 600 to 700 nm. On the other hand, the effects of oxygen saturation are not uniform since oxy-hemoglobin has a unique  $W$  pattern absorption coefficient. When  $S$  increases, the diffuse reflectance decreases from 450 to nearly 500 nm, increases from about 550 to 575 nm, and increases significantly from 600 to 700 nm. This can be explained under the comprehensive absorption of oxy- and deoxy-hemoglobin. From 450 to 500 nm,  $\mu_{a.oxy}$  is larger than  $\mu_{a.deoxy}$ . The absorption is enhanced while  $S$  grows. From 550 to 575 nm and above 600 nm,  $\mu_{a.oxy}$  is smaller than  $\mu_{a.deoxy}$ . Then, we can see that skin diffuse reflectance increases as  $S$  grows.

The thickness of skin layers are also involved and the effects of the thickness of each layer are not the same. Skin diffuse reflectance decreases while  $d_{epi}$  grows. However, it increases while  $d_{der}$ ,  $d_{sub}$  grows. Note that all parameters are initialized as the lower limit. This means the absorption of skin is possibly insufficient and the transmitted light is large. The results may change in realistic condition. Other pigments (e.g. water and fat) are not listed here in this study because they are less weighted in skin absorption given that their absorption coefficients are much smaller than melanin or hemoglobin.

### 3.2 INN Training and Acceleration

We have proved FNN reconstructs extremely similar skin diffuse reflectance to MC. Therefore, another database composed of reflectance spectra from 450 to 700 nm and melanin information was built using FNN for speeding up. 50000 samples were created within 4.3 hours by randomly predefining skin physiological parameters. Note that this second database contains the reflectance spectra but not the reflectance at one wavelength. It took 57 minutes 38 seconds to complete the training process for INN. Moreover, we

applied principal components analysis (PCA) for dimensionality reduction and speeding up. PCA uses orthogonal transformation to linearly transform the observations of a series of possibly related variables, thereby projecting the values of a series of linear unrelated variables. These unrelated variables are called principal components. In our research, we have 50000 observations with 251 variables (from 450 to 700 nm with 1 nm increment), represented by a matrix  $X$  ( $251 \times 50000$ ). Then, a principal components matrix  $Y$  is defined:

$$\begin{aligned} Y^T &= X^T W \\ &= (W D V^T)^T W \\ &= V D^T W^T W \\ &= V D^T \end{aligned} \quad (8)$$

where  $X = W D V^T$  is the singular value decomposition;  $W$  is the eigenvector matrix of  $X X^T$  ( $251 \times 251$ );  $D$  is a  $251 \times 50000$  non-negative rectangular diagonal matrix;  $V$  is the eigenvector matrix of  $X^T X$  ( $50000 \times 50000$ ). We calculated the influence of every principal component and the first seven principal components accounted for above 99.53%. Then, a data matrix  $X$  is transformed to a matrix  $7 \times 50000$  with reduced dimensionality. Another INN was trained based on this low-dimension matrix within 10 minutes 35 seconds.

### 3.3 Verification of Pigments Detection with Synthetic Data

Although our methods give favorable results in regression, to extract or quantify skin physiological parameters, the inverse problem is undoubtedly more important. In other words, our methods need to fit the diffuse reflectance curve precisely without knowing those parameters in prior. The flowcharts of two neural networks are shown in Fig. 5. For FNN, RMSRE between the target and reconstructed diffuse reflectance was reduced until reaching the limits of the optimization process by adjusting the inputs iteratively. In our research, the interior-point algorithm was selected to minimize RMSRE. The maximum number of iterations was assigned to 1000. The initial physiological parameters were randomly set within the proper range and 5 start points were arranged. For INN, we directly obtained the volume fraction of melanin based on inputting the diffuse reflectance spectrum. To validate our methods, we first used 30 samples in three different groups generated by MC as we mentioned above. We first focused on the results of FNN. For lightly pigmented group, satisfactory estimations were obtained for the volume fraction of

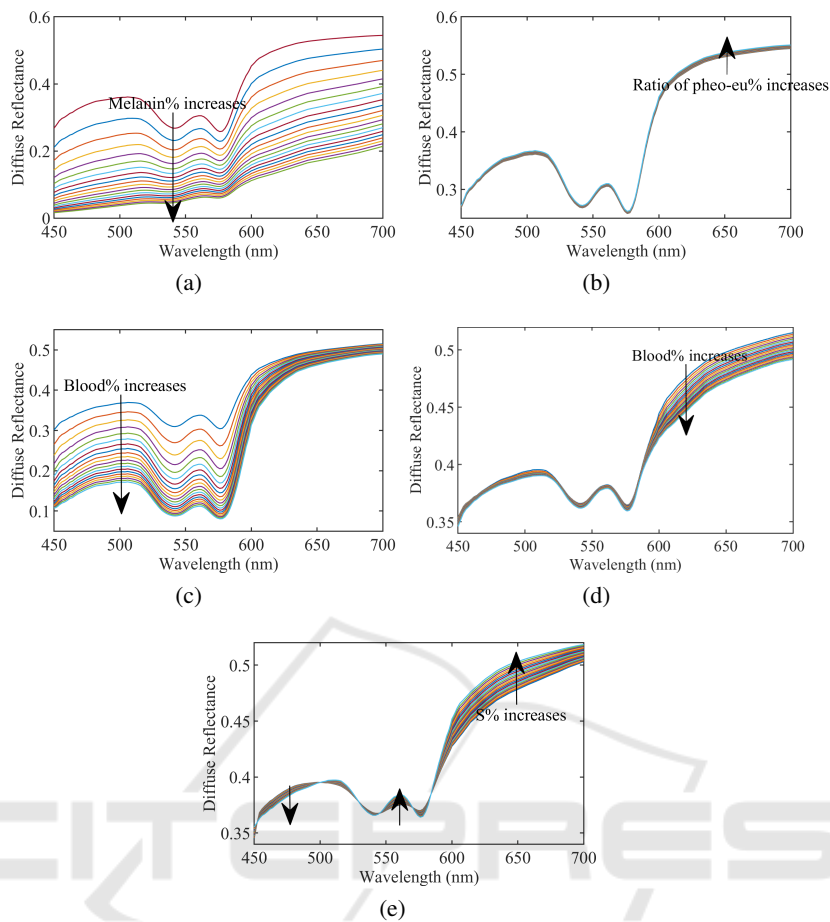


Figure 4: Reconstructing skin diffuse reflectance using varying (a)  $C_m$ ; (b)  $\beta$ ; (c)  $C_{bl\_der}$ ; (d)  $C_{bl\_sub}$ ; (e)  $S$ .

melanin and blood in the dermis, the oxygen saturation, and the thickness of first two layers. Yet not every parameter can be extracted accurately. The rest parameters were not estimated with acceptable errors. Table II shows some estimation results using FNN. The prediction error for the volume fraction of water reaches a maximum of nearly 30%. From the perspective of the absorption coefficients of skin pigments, water is less weighted and has less impact on the diffuse reflectance although its volume fraction is large enough. By contrast, melanin and hemoglobin dominate the light absorption within the skin, thus, the prediction errors are favorable. The situation is quite similar in moderately and darkly pigmented groups. And we find that the estimation of ratio of pheomelanin to eumelanin becomes more accurate when the volume fraction of melanin grows. The average relative errors of  $\beta$  is reduced to almost 5% for darkly pigmented group. Moreover, the thickness of first two layers can be also estimated correctly with the average relative errors 1.11%, 4.80% for  $d_{epi}$  and  $d_{der}$ . The average relative errors of  $C_m$ ,  $C_{bl\_der}$ , and  $S$  for

all three groups are 1.36%, 8.69%, and 3.37% respectively. For the volume fraction of blood in the subcutis and fat, the estimation errors are less than 10%. During this optimization process, the average RMSRE for 30 samples equals to 0.0078, which means FNN can accurately fit the synthetic reflectance curve without knowing skin physiological parameters in prior. Besides, it costs an average of 17 seconds to fit the curve and quantify parameters for one sample. Given that MC needs roughly 332 seconds to reconstruct a spectrum while FNN needs only 0.0019 seconds in our experimentation, using inverse MC probably costs dozens of hours to finish the detection task.

To furthermore speed up the detection, INN was applied to estimate the volume fraction of melanin from 30 samples. Both INN and INN+PCA were tested. Table III gives the detection results for all groups. For lightly pigmented group, the root-mean-square errors (RMSE) and standard deviations (STD) of INN and INN+PCA are  $0.30\% \pm 0.30\%$  and  $0.21\% \pm 0.42\%$  respectively. The small values of RMSE and STD imply that two methods are robust

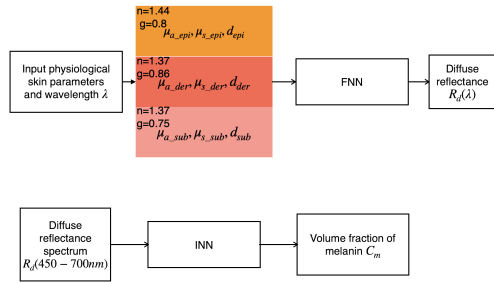


Figure 5: The flowcharts of FNN and INN.

when estimating the volume fraction of melanin. For moderately pigmented group, RMSE and STD of INN and INN+PCA are  $0.40\% \pm 0.39\%$  and  $0.5\% \pm 1.34\%$ . Both two methods have acceptable results and INN becomes more accurate than INN+PCA. For darkly pigmented group, RMSE and STD of INN and INN+PCA are  $2.00\% \pm 1.93\%$  and  $2.33\% \pm 5.6\%$ . The errors become larger but are still acceptable. Given that the target volume fraction of melanin for lightly pigmented group is too low, varying from 1.3% to 3%, the relative errors for this group are the largest among three groups. To sum up, INN and INN+PCA estimate close results for three groups most of time. Although INN is more accurate than INN+PCA, it costs more training time. FNN can estimate precisely not only melanin information but also the oxygen saturation and blood information. However, it costs more time to finish the estimation task while INN and INN+PCA cost only about 0.012 seconds.

### 3.4 Verification of Pigments Detection with Measured Data

Our methods detect several skin physiological parameters successfully from the synthetic diffuse reflectance. The next step is to detect these parameters from the measured data. NIST skin reflectance database was used in this part. The skin diffuse reflectance spectra were acquired with a commercially available spectrophotometer with the help of integrating sphere and this database contains 100 samples with spanning the wavelength range from 250 to 2500 nm with an increment 3 nm (Cooksey et al., 2017). These samples were reshaped using the interpolation algorithm and only the range from 450 to 700 nm was saved for further uses. Afterward, the curve-fitting process was applied and the optimization goal was to minimize RMSRE for FNN and MC. For INN and INN+PCA, they directly detected the melanin information from the target spectrum. Table IV provides the detection results for three samples from NIST database. As we can see, FNN and MC obtained approximate fitting performance. They both need the

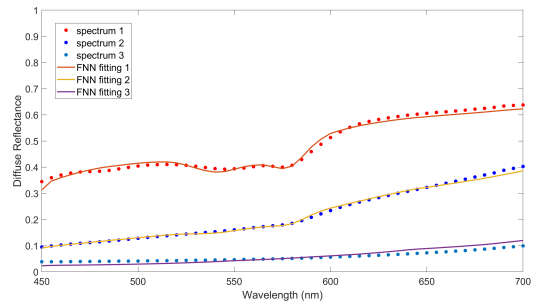


Figure 6: The measured and reconstructed spectra by FNN from NIST.

curve-fitting process to complete the detection task. INN and INN+PCA also obtained approximate values compared to FNN and MC. For spectrum 1, all methods obtained  $C_m$  around 2% which belongs to lightly pigmented group. The estimation results of  $C_{bl\_der}$  and  $S$  are also extremely close for FNN and MC. FNN has a better fitting performance than MC with RM-SRE equals to 2.08%. For the rest two spectra,  $C_m$  were estimated as about 3% and 10%, which matches well the spectra as shown in Fig. 6. In the range from 450 to 700 nm, the diffuse reflectance of spectrum 2 is evenly higher than spectrum 3. Overall, our methods have favorable estimation results in detecting pigments information from the measured spectra.

## 4 DISCUSSION AND CONCLUSION

Our research gives a quantitative analysis of skin based on its diffuse reflectance. MC is used for generating the synthetic training database based on a 3-layered skin model. FNN has been trained to solve the detection task. The absorption of skin is influenced by the combination of various pigments and the thickness of layers. The effects of several skin pigments are analyzed separately. We find that the unique "W" pattern absorption of oxy-hemoglobin can be reflected clearly on the diffuse reflectance spectrum when the absorption of other pigments is not over weighted. The results present that FNN has excellent fitting performance when dealing with synthetic data. And when it comes to the measured data, the fitting performance is also acceptable. The visible light range from 450 to 700 nm is taken into account in our experimentation. As we know, the longer-wavelength light generally has better penetration capacity. The thicker the skin layers, the less likely light will penetrate. A 3-layered skin model is necessary when dealing with thin skin and long-wavelength light. Besides, the pigments detection for melanin and blood in the



Table 2: The fitting results of FNN for one sample in each group.

		$C_m$	$\beta$	$C_{water\_epi}$	$C_{water\_der}$	$C_{water\_sub}$	$C_{bl\_der}$
Sample no.1	Optimized	0.0251	0.0673	0.1496	0.5549	0.6611	0.0623
	Target	0.0251	0.1698	0.1712	0.4724	0.8811	0.0672
Sample no.11	Optimized	0.1577	0.0966	0.1497	0.5545	0.7662	0.0061
	Target	0.1563	0.0870	0.1337	0.6185	0.7512	0.0064
Sample no.21	Optimized	0.2859	0.3380	0.1507	0.6576	0.7755	0.0096
	Target	0.2865	0.3534	0.1607	0.7400	0.8396	0.0102
		$C_{bl\_sub}$	$S$	$C_{fat}$	$d_{epi}$	$d_{der}$	$d_{sub}$
Sample no.1	Optimized	0.0676	0.6508	0.5473	0.0107	0.2574	0.2074
	Target	0.1455	0.6510	0.4865	0.0108	0.2836	0.2381
Sample no.11	Optimized	0.0769	0.5325	0.4702	0.0122	0.0720	0.3485
	Target	0.0560	0.5362	0.4540	0.0124	0.0792	0.2471
Sample no.21	Optimized	0.0566	0.8896	0.5197	0.0116	0.2836	0.1901
	Target	0.0871	0.8854	0.4995	0.0117	0.2627	0.2153

Table 3: Melanin[%] detection results of proposed INN methods for three groups.

Samples	no.1	no.2	no.3	no.4	no.5	no.6	no.7	no.8	no.9	no.10
Target	2.51	2.02	1.76	1.85	2.26	1.74	1.96	1.88	2.79	1.47
INN	2.30	1.78	2.13	1.88	2.41	1.67	1.66	1.30	3.24	1.32
INN+PCA	2.47	1.86	2.23	1.83	2.30	1.56	2.08	1.52	2.78	1.53
Samples	no.11	no.12	no.13	no.14	no.15	no.16	no.17	no.18	no.19	no.20
Target	15.63	12.44	12.18	13.01	13.82	13.48	11.24	14.28	14.45	11.43
INN	15.72	12.59	12.28	12.60	13.77	13.64	12.10	13.89	14.05	11.98
INN+PCA	16.25	12.34	12.29	13.00	13.85	13.41	11.29	14.17	14.42	12.85
Samples	no.21	no.22	no.23	no.24	no.25	no.26	no.27	no.28	no.29	no.30
Target	28.65	24.49	30.97	19.79	36.19	39.78	27.24	28.35	22.17	37.46
INN	28.64	24.01	30.73	19.28	36.14	33.88	27.02	30.42	22.02	37.83
INN+PCA	28.03	24.80	30.69	19.73	35.79	34.91	27.50	33.76	22.35	38.20

dermis (hemoglobin together with the oxygen saturation) are very promising. Other skin physiological parameters like the thickness of each layer are also acceptable. However, for water content, the estimation results are not accurate due to its low light absorption from 450 to 700 nm. This problem may be solved by expanding the light range to infrared where the absorption coefficient of water increases a lot. Moreover, we also introduce INN and PCA to speed up the melanin detection. The accuracy of INN is similar to FNN. INN needs much less computational time than FNN because it doesn't rely on the curve-fitting process. This also makes INN less robust and intuitive than FNN. FNN with the curve-fitting process can reconstruct the diffuse reflectance very well compared with the measured data. As perspectives, we plan to improve our skin model by adding separately upper and deep blood plexus. In tissue, blood is not evenly distributed, but rather confined to vessels (Van Veen et al., 2002). This fact affects the reflectance spectra and is called the vessel packaging effect. The estimation results of the oxygen saturation and the blood can be more accurate with accounting for the vessel packaging. Moreover, the selection of wavelength bands is

also an approach to improve detection performance. For example, we can focus on the "W" pattern range when detecting the oxygen saturation because it is a unique pattern of the absorption coefficient of oxy-hemoglobin. With the development of DRS instruments, we plan to implement FNN and INN to detect skin pigments information non-invasively and in real-time together with the automatic recognition of skin diseases (Carcagnì et al., 2019). This will be much helpful for the quantitative diagnosis of some skin diseases, such as vitiligo and melanoma.

## ACKNOWLEDGEMENTS

We would like to thank China Scholarship Council (CSC) the grant contract number is 201701810030 which partially supports this research.

Table 4: The extracting results of 2L-FANN and 3L-FANN.

Sample	Methods	$C_m$	$C_{bl\_der}$	$S$	$RMSRE$
spectrum 1	FNN	1.31%	0.56%	90.23%	2.08%
	MC	2.13%	0.54%	90.45%	3.28%
	INN	1.84%			
	INN+PCA	1.72%			
spectrum 2	FNN	3.23%	1.02%	94.95%	4.27%
	MC	3.69%	1.08%	94.91%	5.69%
	INN	2.90%			
	INN+PCA	2.87%			
spectrum 3	FNN	10.09%	2.41%	80.00%	10.76%
	MC	9.79%	2.03%	80.02%	8.37%
	INN	10.69%			
	INN+PCA	10.73%			

## REFERENCES

- Alerstam, E., Svensson, T., and Andersson-Engels, S. (2008). Parallel computing with graphics processing units for high-speed monte carlo simulation of photon migration. *Journal of biomedical optics*, 13(6):060504.
- Angelopoulou, E. (2001). Understanding the color of human skin. In *Human vision and electronic imaging VI*, volume 4299, pages 243–251. International Society for Optics and Photonics.
- Baranoski, G. V. and Krishnaswamy, A. (2010). *Light and skin interactions: simulations for computer graphics applications*. Morgan Kaufmann.
- Carcagni, P., Leo, M., Cuna, A., Mazzeo, P. L., Spagnolo, P., Celeste, G., and Distante, C. (2019). Classification of skin lesions by combining multilevel learnings in a densenet architecture. In *International Conference on Image Analysis and Processing*, pages 335–344. Springer.
- Chen, Y.-W., Chen, C.-C., Huang, P.-J., and Tseng, S.-H. (2016). Artificial neural networks for retrieving absorption and reduced scattering spectra from frequency-domain diffuse reflectance spectroscopy at short source-detector separation. *Biomedical optics express*, 7(4):1496–1510.
- Cooksey, C. C., Allen, D. W., and Tsai, B. K. (2017). Reference data set of human skin reflectance. *J. Res. Nat. Inst. Standards Technol.*, 122:1–5.
- Fang, Q. and Boas, D. A. (2009). Monte carlo simulation of photon migration in 3d turbid media accelerated by graphics processing units. *Optics express*, 17(22):20178–20190.
- Flewelling, R. (2000). Noninvasive optical monitoring, in the biomedical engineering handbook, jd bronzino, ed.
- Fredriksson, I., Larsson, M., and Strömberg, T. (2012). Inverse monte carlo method in a multilayered tissue model for diffuse reflectance spectroscopy. *Journal of biomedical optics*, 17(4):047004.
- Furutsu, K. (1980). Diffusion equation derived from space-time transport equation. *JOSA*, 70(4):360–366.
- Ishimaru, A. (1978). *Wave propagation and scattering in random media*, volume 2. Academic press New York.
- Jacques, S. and Prahl, S. Assorted spectra. [EB/OL]. <https://omlc.org/spectra/index.html> Accessed July 15, 2020.
- Jacques, S. L. (1996). Origins of tissue optical properties in the uva, visible, and nir regions. *OSA TOPS on advances in optical imaging and photon migration*, 2:364–369.
- Jacques, S. L. (2013). Optical properties of biological tissues: a review. *Physics in Medicine & Biology*, 58(11):R37–61.
- Jacques, S. L., Glickman, R. D., and Schwartz, J. A. (1996). Internal absorption coefficient and threshold for pulsed laser disruption of melanosomes isolated from retinal pigment epithelium. In *Laser-Tissue Interaction VII*, volume 2681, pages 468–478. International Society for Optics and Photonics.
- Leo, M., Carcagni, P., Mazzeo, P. L., Spagnolo, P., Cazzato, D., and Distante, C. (2020). Analysis of facial information for healthcare applications: A survey on computer vision-based approaches. *Information*, 11(3):128.
- Maeda, T., Arakawa, N., Takahashi, M., and Aizu, Y. (2010). Monte carlo simulation of spectral reflectance using a multilayered skin tissue model. *Optical review*, 17(3):223–229.
- Mazzoli, A., Munaretto, R., and Scalise, L. (2010). Preliminary results on the use of a noninvasive instrument for the evaluation of the depth of pigmented skin lesions: numerical simulations and experimental measurements. *Lasers in medical science*, 25(3):403–410.
- Mehrübeoğlu, M., Kehtarnavaz, N., Marquez, G., Duvic, M., and Wang, L. V. (2002). Skin lesion classification using oblique-incidence diffuse reflectance spectroscopic imaging. *applied optics*, 41(1):182–192.
- Naglič, P., Vidovič, L., Milanič, M., Randeberg, L. L., and Majaron, B. (2019). Suitability of diffusion approximation for an inverse analysis of diffuse reflectance spectra from human skin in vivo. *Osa Continuum*, 2(3):905–922.
- Parsad, D., Wakamatsu, K., Kanwar, A., Kumar, B., and Ito, S. (2003). Eumelanin and pheomelanin contents of

- depigmented and repigmented skin in vitiligo patients. *British Journal of Dermatology*, 149(3):624–626.
- Salomatina, E. V., Jiang, B., Novak, J., and Yaroslavsky, A. N. (2006). Optical properties of normal and cancerous human skin in the visible and near-infrared spectral range. *Journal of biomedical optics*, 11(6):064026.
- Sharma, M., Hennessy, R., Markey, M. K., and Tunnell, J. W. (2014). Verification of a two-layer inverse monte carlo absorption model using multiple source-detector separation diffuse reflectance spectroscopy. *Biomedical optics express*, 5(1):40–53.
- Spott, T. and Svaasand, L. O. (2000). Collimated light sources in the diffusion approximation. *Applied optics*, 39(34):6453–6465.
- Tsui, S.-Y., Wang, C.-Y., Huang, T.-H., and Sung, K.-B. (2018). Modelling spatially-resolved diffuse reflectance spectra of a multi-layered skin model by artificial neural networks trained with monte carlo simulations. *Biomedical optics express*, 9(4):1531–1544.
- Van Veen, R., Verkruijse, W., and Sterenborg, H. (2002). Diffuse-reflectance spectroscopy from 500 to 1060 nm by correction for inhomogeneously distributed absorbers. *Optics letters*, 27(4):246–248.
- Vyas, S., Banerjee, A., and Burlina, P. (2013). Estimating physiological skin parameters from hyperspectral signatures. *Journal of biomedical optics*, 18(5):057008.
- Wallace, V., Crawford, D., Mortimer, P., Ott, R., and Bamber, J. (2000). Spectrophotometric assessment of pigmented skin lesions: methods and feature selection for evaluation of diagnostic performance. *Physics in Medicine & Biology*, 45(3):735.
- Wang, L., Jacques, S. L., and Zheng, L. (1995). Monte carlo modeling of light transport in multi-layered tissues. *Computer methods and programs in biomedicine*, 47(2):131–146.
- Wang, Q., Le, D., Ramella-Roman, J., and Pfefer, J. (2012). Broadband ultraviolet-visible optical property measurement in layered turbid media. *Biomedical optics express*, 3(6):1226–1240.
- Yudovsky, D. and Durkin, A. J. (2011). Spatial frequency domain spectroscopy of two layer media. *Journal of biomedical optics*, 16(10):107005.
- Yudovsky, D., Nguyen, J. Q. M., and Durkin, A. J. (2012). In vivo spatial frequency domain spectroscopy of two layer media. *Journal of biomedical optics*, 17(10):107006.
- Zerbino, D. (1994). Biopsy: its history, current and future outlook. *Likars' ka sprava*, (3-4):1–9.
- Zhang, L., Wang, Z., and Zhou, M. (2010). Determination of the optical coefficients of biological tissue by neural network. *Journal of Modern Optics*, 57(13):1163–1170.
- Zherebtsov, E., Dremin, V., Popov, A., Doronin, A., Kurakina, D., Kirillin, M., Meglinski, I., and Bykov, A. (2019). Hyperspectral imaging of human skin aided by artificial neural networks. *Biomedical optics express*, 10(7):3545–3559.
- Zonios, G., Dimou, A., Bassukas, I., Galaris, D., Tsolakidis, A., and Kaxiras, E. (2008). Melanin absorption spectroscopy: new method for noninvasive skin investigation and melanoma detection. *Journal of biomedical optics*, 13(1):014017.